



HAL
open science

OC6 Phase I: Investigating the underprediction of low-frequency hydrodynamic loads and responses of a floating wind turbine

A. N. Robertson, S. Gueydon, E. Bachynski, L. Wang, J. Jonkman, D. Alarcón, E. Amet, A. Beardsell, P. Bonnet, B. Boudet, et al.

► To cite this version:

A. N. Robertson, S. Gueydon, E. Bachynski, L. Wang, J. Jonkman, et al.. OC6 Phase I: Investigating the underprediction of low-frequency hydrodynamic loads and responses of a floating wind turbine. *Journal of Physics: Conference Series*, 2020, 1618, pp.032033. 10.1088/1742-6596/1618/3/032033 . hal-03007787

HAL Id: hal-03007787

<https://ifp.hal.science/hal-03007787>

Submitted on 16 Nov 2020

HAL is a multi-disciplinary open access archive for the deposit and dissemination of scientific research documents, whether they are published or not. The documents may come from teaching and research institutions in France or abroad, or from public or private research centers.

L'archive ouverte pluridisciplinaire **HAL**, est destinée au dépôt et à la diffusion de documents scientifiques de niveau recherche, publiés ou non, émanant des établissements d'enseignement et de recherche français ou étrangers, des laboratoires publics ou privés.



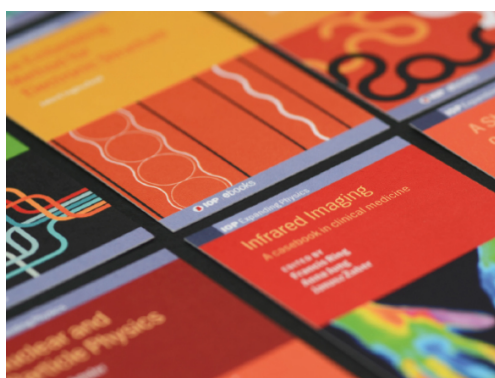
Distributed under a Creative Commons Attribution 4.0 International License

PAPER • OPEN ACCESS

OC6 Phase I: Investigating the underprediction of low-frequency hydrodynamic loads and responses of a floating wind turbine

To cite this article: A N Robertson *et al* 2020 *J. Phys.: Conf. Ser.* **1618** 032033

View the [article online](#) for updates and enhancements.



IOP | ebooks™

Bringing together innovative digital publishing with leading authors from the global scientific community.

Start exploring the collection—download the first chapter of every title for free.

OC6 Phase I: Investigating the underprediction of low-frequency hydrodynamic loads and responses of a floating wind turbine

A N Robertson¹, S Gueydon², E Bachynski³, L Wang¹, J Jonkman¹, D Alarcón⁴, E Amet⁵, A Beardsell⁶, P Bonnet⁷, B Boudet⁵, C Brun⁸, Z Chen⁹, M Féron¹⁰, D Forbush¹¹, C Galinos¹², J Galvan¹³, P Gilbert¹⁴, J Gómez¹⁵, V Harnois¹⁵, F Haudin¹⁶, Z Hu¹⁷, J Le Dreff¹⁸, M Leimeister¹⁹, F Lemmer²⁰, H Li³, G McKinnon²¹, I Mendikoa¹³, A Moghtadaei²², S Netzband²³, S Oh²⁴, A Pegalajar-Jurado¹², M Q Nguyen¹⁶, K Ruehl¹¹, P Schünemann²⁵, W Shi²⁶, H Shin²⁷, Y Si⁹, F Surmont⁸, P Trubat⁴, J Qwist²⁸, S Wohlfahrt-Laymann²⁰

¹National Renewable Energy Laboratory, 15013 Denver W Pkwy, Golden, CO, USA 80401

²Maritime Research Institute Netherlands, Haagsteeg 2, 6708 PM Wageningen, Netherlands

³Norwegian University of Science and Technology, 7491 Trondheim, Norway

⁴Universitat Politècnica de Catalunya, Jordi Girona 1-3, 08034, Barcelona, Spain

⁵Bureau Veritas, 60 avenue du Général de Gaulle, 92046 Paris - La Défense

⁶DNV GL, One Linear Park, Avon St., Temple Quay, Bristol, BS2 0PS, UK

⁷Siemens Digital Industries Software, C/Lluis Muntadas 5, Cornellà, Spain 08940

⁸Bureau Veritas, 8, avenue Jacques Cartier, Atlantis - 44807 Saint-Herblain Cdx - France

⁹Ocean College, Zhejiang University, Zhoushan 316021, China

¹⁰DORIS Engineering, 58a rue du Dessous des Berges, 75013 Paris, France

¹¹Sandia National Laboratories, 1515 Eubank Blvd SE, Albuquerque, NM 87123

¹²DTU Wind Energy, Nils Koppels Allé 403, Kgs. Lyngby, DK-2800, Denmark

¹³Tecnalia Research & Innovation, Parque Tecnológico Bizkaia, Ed.700, 48160 Derio, Spain

¹⁴IFPEN, 4 avenue de Bois Préau 92852 Rueil-Malmaison Cedex, France

¹⁵PRINCIPIA, ZAC Athelia I - 215 Voie Ariane, 13705 La CIOTAT Cedex France

¹⁶Vulcain Ingénierie, 5 rue Beffroy, 92200 Neuilly-sur-Seine, France

¹⁷School of Engineering, Newcastle University, Newcastle upon Tyne, NE1 7RU, UK

¹⁸EDF R&D, 7 boulevard Gaspard Monge, 91120 Palaiseau, France

¹⁹Fraunhofer Inst. for Wind Energy Systems, Am Luneort 100, 27572 Bremerhaven, Germany

²⁰University of Stuttgart, 70569 Stuttgart, Germany

²¹Orcina Ltd., Daltongate, Ulverston, Cumbria LA12 7AJ, UK

²²Queen's University Belfast, Belfast, BT9 5AG, Northern Ireland, United Kingdom

²³Hamburg University of Technology, 21071 Hamburg, Germany

²⁴ClassNK, 4-7 Kioicho, Chiyodaku, Tokyo, Japan

²⁵Universität Rostock, Albert-Einstein-Str. 2, 18059 Rostock, Germany

²⁶Dalian University of Technology, No.2 Linggong Road, Dalian, Liaoning, China 116024

²⁷University of Ulsan, 93 Daehakro Namgu Ulsan, 44610, South Korea

²⁸Subsea, Hagaløkkveien 26, 1383 Asker, Norway

Amy.Robertson@nrel.gov

Abstract. Phase I of the OC6 project is focused on examining why offshore wind design tools underpredict the response (loads/motion) of the OC5-DeepCwind semisubmersible at its surge and pitch natural frequencies. Previous investigations showed that the underprediction was primarily related to nonlinear hydrodynamic loading, so two new validation campaigns were performed to separately examine the different hydrodynamic load components. In this paper, we



validate a variety of tools against this new test data, focusing on the ability to accurately model the low-frequency loads on a semisubmersible floater when held fixed under wave excitation and when forced to oscillate in the surge direction. However, it is observed that models providing better load predictions in these two scenarios do not necessarily produce a more accurate motion response in a moored configuration.

1. Introduction

Currently, floating wind systems are in a precommercial stage of development with one five-turbine wind farm and some single utility-scale prototypes deployed in the open ocean. Fixed-bottom systems are becoming quite prolific, in large part due to their competitive cost of energy. Floating wind systems, however, are still significantly more expensive, and the costs for these systems need to be reduced to be commercially viable. That cost reduction will come from a variety of sources: One avenue is to better optimize the designs to minimize the requirements on support structures and make them easier to mass manufacture and deploy. Floating wind optimization is difficult because the systems are complex and coupled, with multiple sources of excitation. An efficient search for optimal solutions requires advanced modeling and design tools capable of accurately capturing the physical behavior of these systems under realistic conditions. Methodically identifying and addressing the sources of inaccuracy and uncertainty in these tools will enable a path toward finding cost-optimal floating wind design solutions.

The OC3 (Offshore Code Comparison Collaboration) – OC6 projects (Offshore Code Comparison Collaboration, Continued with Correlation and unCertainty) were created under the framework of the International Energy Agency (IEA) Wind to address the need for verifying and validating the load predictions of coupled modeling tools for offshore wind design. In the present phase (Phase I of OC6), the focus is on examining the underprediction of the response (loads/motion) of a floating semisubmersible (semi) at its surge and pitch natural frequencies. This issue was identified within the OC5 Phase II project [1], which focused on validating modeling tools against a scaled-model test of the OC5-DeepCwind semi in a wave tank under combined wind and wave loading. In general, the modeling tools represented the behavior of the system well, but with a persistent underprediction of the global loads and motion (about 20% underprediction). In some applications this level of inconsistency would be considered acceptable; however, it is a concern when attempting to develop optimized designs. Further investigation showed that the underprediction came primarily from the underestimation of the loads/motion of the semi in the low-frequency region where the pitch and surge natural frequencies were located. These frequencies lie outside the linear wave excitation region and are excited by nonlinear hydrodynamic loading.

The underprediction of the response of floating wind systems at these frequencies has been reported by other researchers as well. Azcona et al. [2] investigated new hybrid techniques for wind loading on floating systems and found that, even when wind loading was included, the low-frequency response of a semi (similar to the present geometry) was underpredicted when comparing simulations to experimental measurements. Pegalajar-Jurado and Bredmose [3] investigated methods to better represent the low-frequency response of the NAUTILUS-DTU10 floating wind turbine (a semi design) by tuning damping values directly from a sea state using operational modal analysis. They found that tuning the damping to the response under irregular or random (pink noise) wave loading led to a better match as compared to tuning the damping properties from free-decay tests. However, the tuning had to be redone for each wave case. Simos et al. [4] investigated various frequency-domain formulations for predicting the low-frequency response of a semi in irregular waves, paying special attention to the effect of quadratic transfer functions (QTFs). By comparing the model predictions with

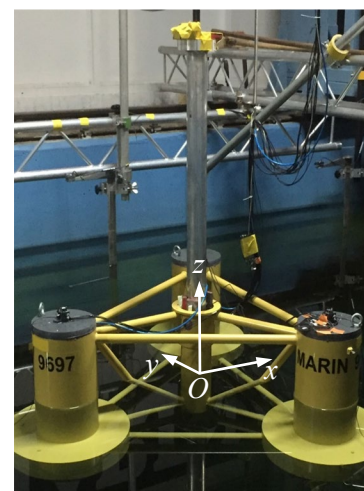


Figure 1: Configuration 1, OC6-DeepCwind floating semi-submersible with rigid tower (photo by Amy Robertson, NREL)

wave-tank experiments, it was observed that Newman's approximation tends to underestimate the second-order response in some cases. Underprediction at low frequencies has even been seen in tension-leg-platform designs, as highlighted in Caillé et al [5]. Some success in this area was achieved by Lemmer et al. [6] when examining the TripleSpar floating wind system. The authors were able to reproduce the surge, heave, and pitch low-frequency response in irregular waves using drag values from the literature. The reason for the improved results is believed to be related to the fact that the heave plates are located quite deep (54 m), compared to about 20 m for the OC5-DeepCwind semi.

2. Methodology

To better understand the nonlinear hydrodynamic loading, two new wave-tank validation campaigns were performed at the concept basin at MARIN for the OC5-DeepCwind semisubmersible design. Phase I of OC6 is dedicated to validating simulation models using the measurements from these experiments to better understand the reasons for the underprediction of the nonlinear hydrodynamic response.

In the first campaign, the floating system was simplified from the testing configuration in OC5 to remove as much uncertainty from the test as possible. Since hydrodynamic loads were of primary interest, the turbine was removed and the tower was changed to a stout, rigid one with inertial properties similar to those of the OC5-DeepCwind semi turbine and tower combined (see Figure 1, Configuration 1). The mooring system was also replaced with a spring and wire mooring system that reproduced the angle at the fairlead and the linear response behavior of the original catenary system (see [7, 8] for more details). The wetted geometry in the tests was the same as for the OC5 system. The 6-degree of freedom (DOF) motion of the system, the mooring loads at each fairlead, and the wave elevation at multiple locations were measured. Through extensive repetition tests and documentation of sources of uncertainty bias, the first campaign assessed the role of uncertainty in the experiments in the disparity between simulations and measurements.

The second validation campaign [8] investigated the diffraction and radiation hydrodynamic loads on the floating wind system separately. The tower was removed from the floater and the platform was affixed to a carriage system as shown in Figure 2 (Configuration 2). This setup allowed the floater to be held fixed under wave excitation to examine the diffraction loads, then to be forced to oscillate in the surge direction to examine the radiation loads. Of course, for both conditions, drag forces were still present as well. The 6-DOF force on the entire structure was measured at the top of the structure, and the same wave cases from the previous campaign were run for this configuration. The right-handed coordinate system used in this study originates on the calm water level at the center of the central column, with positive x (surge) in the direction of wave propagation and z upward (see Figure 1).

The five load cases (LC) examined in the two experimental campaigns are summarized in **Table 1**. All data and results are presented at full scale. The details of the most relevant cases are provided in **Table 2** and **Table 3**. A full summary of the system properties for the two configurations and the associated load cases can be found in the description document for the project [8].



Figure 2: Configuration 2, OC6-DeepCwind floating semisubmersible attached to a carriage – seen from +x to -x (photo by Amy Robertson, NREL)

Table 1. Load Case Configurations

Load Case	Configuration	Description
LC 1	Configuration 2	Towing tests at 6 velocities: 0.5, 1.0, 1.5, 2.0, 2.5, and 3.0 m/s
LC 2	Configuration 2	Forced surge oscillation at 3 frequencies, each with 2 amplitudes
LC 3	Configuration 2	Four wave cases—2 regular and 2 irregular
LC 4	Configuration 1	Free decay in 3 DOFs with 2 initial offset positions for each DOF
LC 5	Configuration 1	Four wave cases—same as for LC 3

Table 2. Specification of Forced Oscillation and Free-Decay Load Cases

Load Case	Amplitude (m)	Period (s)	Load Case	Mode	Initial Offset
2.1	40.11	105.2	4.1	Surge	-1.86 m
2.2	30.07	104.5	4.2	Surge	-3.39 m
2.3	9.601	31.23	4.3	Heave	-1.06 m
2.4	6.444	31.01	4.4	Heave	-1.57 m
2.5	3.367	21.07	4.5	Pitch	-2.21°
2.6	4.481	21.02	4.6	Pitch	-3.95°

Table 3. Irregular Wave Specification

Load Case	Spectrum	Significant Wave Height (m)	Peak Period (s)	Simulation Length
3.3 and 5.3	JONSWAP, $\gamma=3.3$	7.4	12.0	3 hr
3.4 and 5.4	White Noise	6.7	6-26	3 hr

Participants of the OC6 project built numerical models for the two configurations (fixed and floating) in their respective tools and simulated the five load cases in the time domain. The modeling approaches used by the participants are summarized in the Appendix. Participants used either a potential flow (PF)-based solution, a strip-theory solution with Morison's equation, or a combination of the two. The potential-flow models use radiation/diffraction matrices computed from a frequency-dependent boundary-element method (BEM), such as WAMIT. To account for viscous effects, some participants added the drag term from Morison's equation to their time-domain solution, whereas others added a damping matrix ("Additional Damping" in the Appendix) in place of, or in addition to, this drag term. For the BEM solution, some participants used only a first-order solution; those using a second-order solution included the QTF. To evaluate the QTF, it is necessary to solve the second-order potential-flow problem where the boundary condition on the body surface depends on the first-order motion of the floater. Therefore, most models based on second-order PF used two sets of QTFs: one for the fixed condition (LC 3.3) and another for the floating condition (LC 5.3). One exception is NTNU which used the QTF for the floating condition in both cases. Other modeling choices that contribute to the response are wave stretching and the use of measured waves from the experiment instead of synthetic waves with the appropriate spectrum.

Results for LC 1-4 were provided to the participants to tune their models. The exact tuning approach differs for each participant; however, most focused on adjusting the drag coefficients to match the steady drag and moment of LC 1 and/or the radiation load of LC 2. Some also tuned damping matrices based on the free-decay time history of LC 4. It should be noted that the participants were required to produce reasonable predictions at the wave frequencies for LC 3; tuning purely for low frequencies at the expense of wave-frequency response was not allowed. LC 5 was reserved for a "blind comparison." Only those that worked on the experiments, NREL and the Norwegian University of Science and Technology, had access to the experimental data of LC 5, though their models were not calibrated based on this load case.

The validation approach taken in this project was to determine whether simulated results using a model with the measured properties of the experiment fall within the uncertainty bounds of the experimental measurements. These bounds encompassed uncertainties in the measurement sensors as well as the excitation to the system (e.g., wave properties) and the system properties (e.g., mass/inertia and mooring properties). The uncertainty of the excitation and system properties were propagated to the system response and combined with the measurement uncertainty, as summarized by Robertson et al. [7]. An alternative approach would be to put the excitation and system uncertainties on the modeling side; however, the approach used here allowed for a more straightforward assessment of validation.

To validate the simulation response for these load cases against the measurements, a "PSD sum" metric was created to capture frequency-dependent responses both inside and outside the wave

frequency range of irregular sea states. The power-spectral density (PSD) sums are computed based on the one-sided, unsmoothed, discrete power density functions:

$$S_{sum} = \sum_{i=j}^k S_{resp}(f_i) \Delta f$$

where $S_{resp}(f_i)$ is the discrete PSD of the response at frequency f_i , Δf is the frequency increment, j and k are the indices of the first and last frequency of interest. The frequency limits for the low- and wave-frequency regions of the spectrum are shown in **Table 4**. These are based on identifying the ranges over which the wave spectra were defined, then encompassing the lower frequencies below that range without considering the zero-frequency mean value.

Table 4. Frequency Limits for Summation of Power Spectral Density for Response Metrics

Wave	Low-Frequency Window	Wave-Frequency Window
Irregular Wave	0.005 to 0.05 Hz	0.05519 to 0.1345 Hz
White Noise	0.005 to 0.036 Hz	0.0385 to 0.1667 Hz

3. Results

The validation objective for this work is to accurately predict the low-frequency response of the floating semi under irregular wave loading in LC 5.3 and 5.4, which correspond to a JONSWAP and white-noise wave, respectively. The results presented here, however, only focus on LC 5.3 because of the limitations on paper length. Validation is achieved if the PSD sum metric in the low-frequency region (see Table 4) of the simulated results falls within the uncertainty bounds of the experimental measurements. LC 2, 3, and 4 are used to examine the ability of the simulation tools to predict the hydrodynamic load components that contribute to the floating response in LC 5. LC 1 did not provide much insight into the predictions for a floating configuration and, therefore, is not included in the analysis in this paper.

A comparison of the PSD of the surge response for LC 5.3 (floating platform) and the surge force for LC 3.3 (fixed platform) between simulations and experiment is shown in **Figure 3**. The PSD sum metric ranges are indicated by the pink coloration for the low-frequency region and blue for the wave frequency. Both figures show a large response peak at the wave frequency around 0.08 Hz; however, the floating condition (LC 5.3) also shows a larger peak in the low-frequency region associated with the surge natural frequency of the system at approximately 0.01 Hz. With only a few exceptions, most participants (shown in different colors) match the experimental measurements (ZXP0 shown in black) in the wave-frequency region well, but underestimate the load/motion in the low-frequency region both for the fixed (LC 3) and floating (LC 5) conditions. The goal here is to understand the source of the differences between simulation and experiment for the surge natural frequency peak in LC 5.3 as well as the pitch natural frequency peak for the pitch response (shown in **Figure 4**).

Figure 5 shows the PSD sum metric for the surge loads and motion across LC 2, 3, and 5. As shown in **Figure 5c**, no modeling tool was able to predict the response at the surge natural frequency for LC 5.3 within the uncertainty bounds of the experiment (grey bands); therefore, all simulation tools fail the validation objective. The hatched bars indicate modeling tools that use a Morison's equation-only approach, and those with a red dot indicate a second-order PF solution. For LC 2, 3, and 5, the simulation results are sorted from highest to lowest values.

In the engineering tools, the forces that affect the motion at the natural frequencies include, among others, the wave and viscous excitation on a fixed system (modeled in LC 3.3 – **Figure 5b**) as well as the radiation and viscous drag associated with a moving structure (modeled in LC 2.1 – **Figure 5a**). For LC 2.1, many tools underpredict the force during oscillation, mostly due to an underprediction of radiation and/or viscous drag (the force component in phase with surge velocity). The higher predictions are mainly attributed to a higher-valued transverse drag coefficient. The underprediction of the surge force (F_x) on a fixed structure under wave loading (**Figure 5b**) is more significant. **Figure 3** shows that the force levels in the low-frequency region for this configuration are small, but they nevertheless can contribute to large resonant responses. Those modeling approaches that result in a larger value than others for the fixed-condition surge force are again those that utilize an increased drag coefficient and

those that incorporate a second-order PF solution. DTU1 is the only Morison-only approach predicting a large surge force in **Figure 5b**, likely because of the use of fully nonlinear wave kinematics, which are not used in other Morison-only models. In the DTU1 model, the measured time series of the free-surface elevation were band-pass filtered to remove sub- and super-harmonic content to obtain the target “linear” wave signal at the floater location. A fully nonlinear wave model was then used to furnish the filtered wavefield with additional nonlinear components. This approach provided the simulation with fully nonlinear fluid velocity and acceleration of the incident wavefield which likely improved the accuracy of Morison added-mass and drag forces.

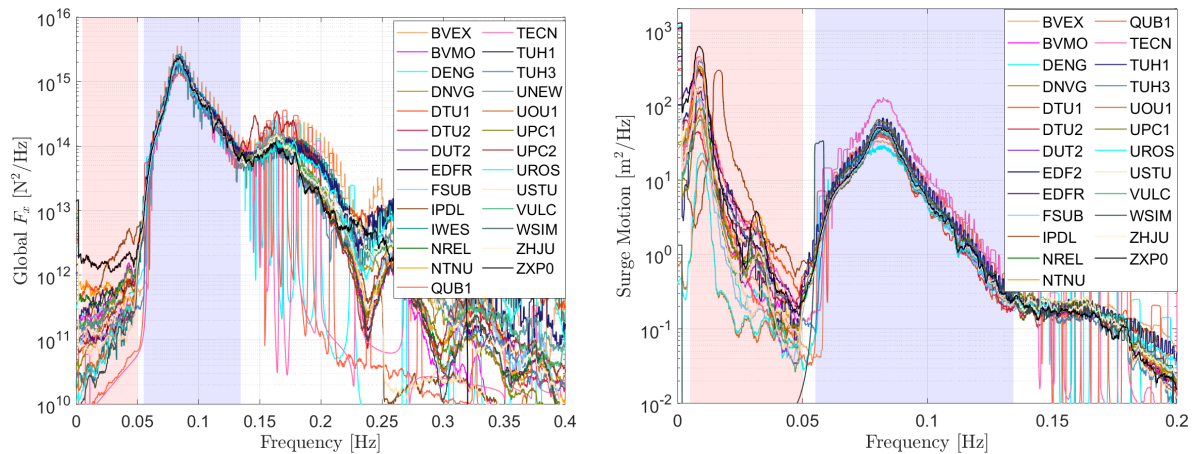


Figure 3. PSD comparison of experimental measurement to simulations for the surge force for LC 3.3 and surge response for LC 5.3.

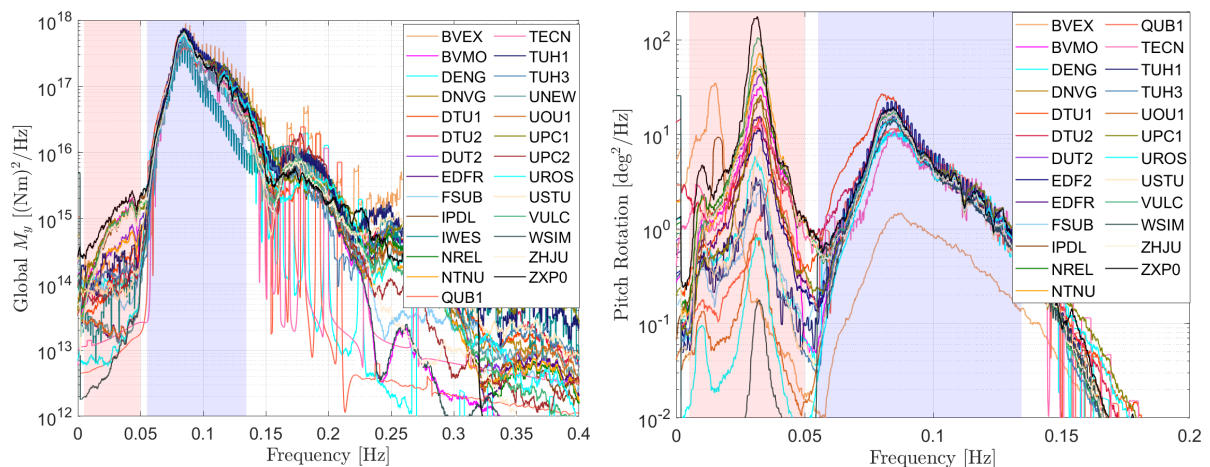


Figure 4. PSD comparison of experimental measurement to simulations for the pitch moment for LC 3.3 and pitch response for LC 5.3.

However, larger surge forces in LC 2.1 and LC 3.3 at the low frequencies do not equate to a larger surge response at the surge natural frequency for LC 5.3. Instead, those that have the largest response (e.g., TECN, EDFR, TUH3, and USTU) have some of the smallest forces for LC 2.1 and 3.3. To try to better understand the reason for higher response levels in LC 5.3, one can also look at the behavior of the model in free decay (LC 4). The linear and quadratic damping, represented by P and Q values [9] derived from surge-free decay time history of the floating system (LC 4.2), are summarized in **Figure 5d** and **5e**. The large linear damping from the experiment is significantly higher than what PF wave radiation models would suggest, forcing many participants to add strong external linear damping to the model that is not flow dependent. TECN, EDFR, TUH1 (same as the TUH3 model), and USTU are among the exceptions that did not use any additional damping, resulting in negligible linear damping.

Therefore, larger drag coefficients and added damping matrices, while providing a better match for fixed-condition loads and free-decay characteristics, generally fail to produce better estimation of the floating response at the surge natural frequency. The resolution of this conflict requires a better understanding of the source of the large linear damping observed in the experiment. It may come from the unsteady drag, which might not be quadratic in nature, or from a more complicated mechanism where viscous effects alter the wave radiation characteristics of the platform. Again, DTU1 stands out by predicting large surge motion despite the use of external damping and a large drag coefficient. The use of fully nonlinear wave kinematics likely improved the motion prediction.

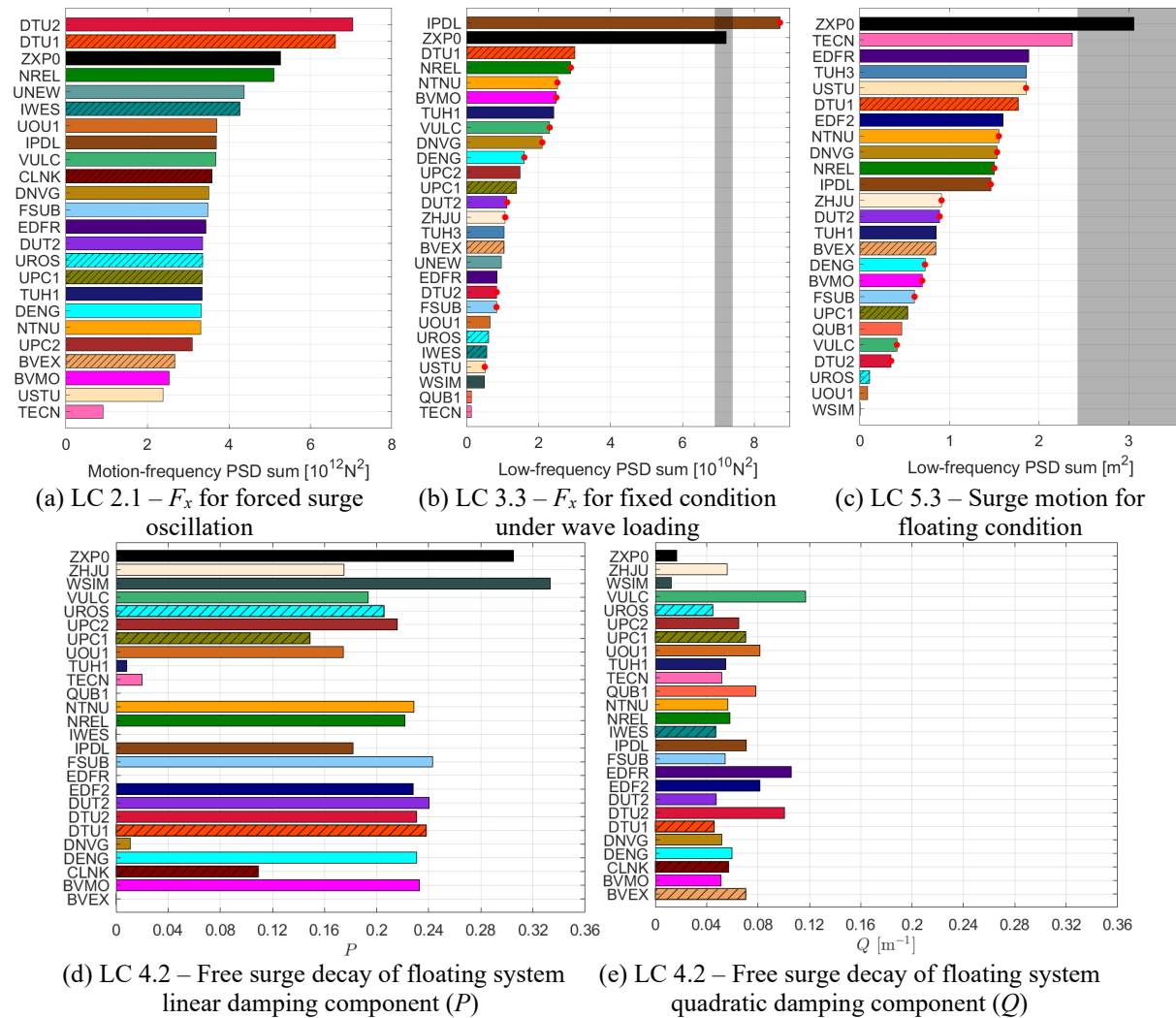


Figure 5. Comparison of surge-frequency-related hydrodynamic loads and motion (LC 2.1, 3.3, 5.3, and 4.2). PSD sum in (a) were computed over a frequency range $\pm 10\%$ of the motion frequency. P and Q shown in (d) and (e) are proportional to the linear and quadratic damping coefficients.

For PF models, the features that consistently improve the result across load cases are the inclusion of a QTF from second-order PF solutions and the use of measured waves from the basin. The measured waves contain some low-frequency components absent from the target wave spectra, creating additional excitation at low frequencies. To provide an estimate of the contribution from these low-frequency wave components, the NREL model, which constructed the wavefield using linear superposition based on the measured waves, was run a second time with low-frequency wave components removed. More specifically, the original measured waves were filtered by zeroing all frequency components below 0.05 Hz. With the filtered waves as input, the low-frequency PSD sums for surge force and pitch moment (**Figure 5b** and **6b**) predicted by the NREL model were reduced by 25% and 10%, respectively. In

addition to the use of QTF and measured waves, wave stretching, to a lesser degree, also tends to improve the result. With Morison-only models, the use of fully nonlinear wave kinematics coupled with large drag coefficients appears to provide significantly improved predictions for surge force and motion.

Figure 6 shows the same analysis of the *pitch* load/response of the floating wind system in irregular waves. Again, it is shown in **Figure 6c** that none of the modeling tools are able to predict the low-frequency response accurately. For LC 2.1 (**Figure 6a**), the forced oscillation is still in the surge direction, but the pitch moment (M_y) is examined. The results here are fairly similar to those observed for the surge forces. However, for LC 3.3, a different group of models perform better for the pitch moment. The Morison-only model DTU1 that predicted the surge force well largely underpredict the pitch moment. This observation also holds for LC 5.3 where no Morison-only model is in the top tier for response prediction.

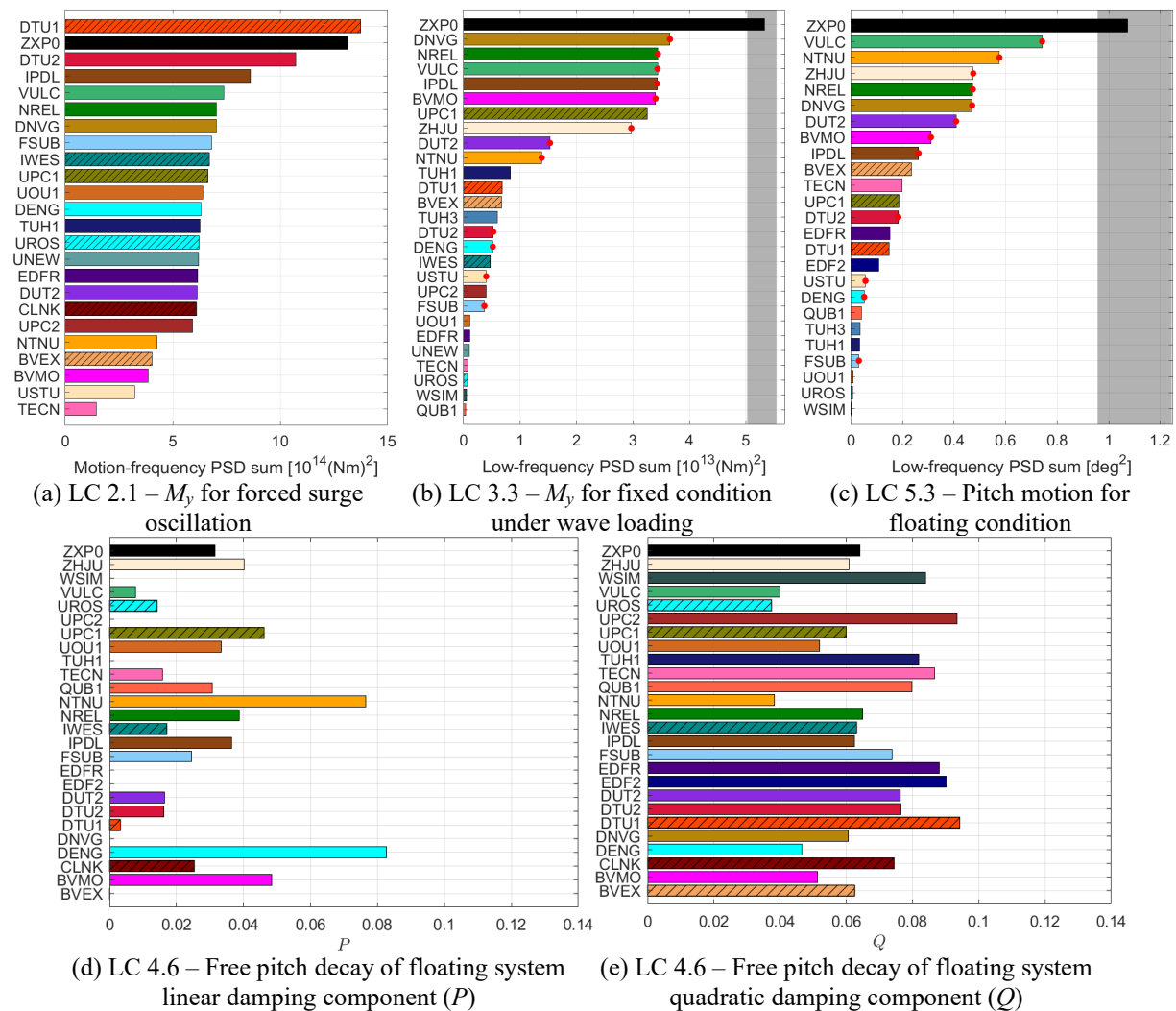


Figure 6. Comparison of pitch-frequency-related hydrodynamic loads and motion (LC 2.1, 3.3, 5.3, and 4.6). PSD sum in (a) were computed over a frequency range $\pm 10\%$ of the motion frequency. P and Q shown in (d) and (e) are proportional to the linear and quadratic damping coefficients.

The damping characteristics in the pitch direction are also very different than for surge. In surge, the linear damping dominates over the quadratic. For the pitch direction, however, the linear damping is much smaller while quadratic damping becomes significant, indicating the importance of viscous drag across the heave plates. The damping behavior influences the pitch response for LC 5.3. Notice that the lack of added linear damping no longer produces a larger response in pitch. Otherwise, it is hard to identify any common components that lead to a larger pitch response other than the two features that are

shown to consistently improve the result across all load cases: the inclusion of a QTF for second-order PF solutions and the use of measured waves from the basin. It should be noted that DENG, FSUB, and USTU all use Newman's approximation instead of the full QTF, which likely caused the low pitch moment in **Figure 6b** [4].

Another approach that has been shown to improve the pitch-moment prediction under some conditions is to use distinct drag coefficients for different parts of the platform (e.g., see [10]). Since engineering-level modeling tools do not account for the flow acceleration around the bottom of the platform, one can tune the drag coefficient to approximate the effect. This modeling approach worked well for LC 1 where the structure was towed at different velocities and, to a lesser degree, LC 2 with forced surge oscillation. However, the benefit is not obvious under floating conditions.

4. Conclusions

OC6 Phase I sought to better understand the source of the underprediction of the response of floating semisubmersibles at their surge and pitch natural frequencies. This underprediction was found to have a significant impact on the accurate prediction of the ultimate and fatigue loads of floating wind systems.

As part of the project, a set of experiments was performed to break apart the low-frequency loads to understand the source of the underprediction. Constrained tests were performed to examine the radiation and viscous loading under forced surge oscillation, then the diffraction and viscous loading in a fixed condition under waves. For both test conditions, the modeling tools in general under-predicted both the surge force and pitch moment, resulting in the underprediction of the floating response at the natural frequencies.

For PF models, a few model features were shown to consistently improve the match to experimental measurements across load cases. First is the inclusion of second-order PF solutions in the form of a QTF that models the difference-frequency inviscid wave loading on the system. The second component is the use of measured waves, which contains some lower-frequency content absent from the target wave spectra. However, without a better understanding of the nature of the measured low-frequency waves, it is difficult to determine whether the wave nonlinear effect is double counted in this case.

Morison-only solutions tend to work relatively well in surge, especially when fully nonlinear wave kinematics are used, but underpredict pitch load and motion at the pitch natural frequency. The use of fully nonlinear wavefield can be highly beneficial to Morison-only models because it improves the evaluation of the added-mass component with more accurate flow acceleration. The accuracy of the drag component may also be improved; however, this is likely less important since the Morison drag, up to second order, only depends on the first order wavefield velocity.

Wave stretching also improves the surge predictions, but not pitch. The damping models have a significant effect on the response of the system. Larger drag coefficients and external damping matrices lead to larger forces for the constrained configuration that better match the experimental measurements. Many participants set these damping values based on the free-decay response of the experiment. However, the increased drag and damping tend to decrease the motion response of the system under wave excitation, increasing the discrepancy with experiment for these cases. This contradiction seems to indicate that some flow mechanism is missing from the models that are being used.

One idea to improve the models is to have a viscous drag coefficient that is frequency and/or amplitude-dependent; however, that can be difficult to formulate for an irregular sea state where multiple frequency components with different amplitudes coexist. Furthermore, we observe that in a fixed condition, the surge force is being underpredicted. Therefore, perhaps the PF QTF itself needs to be corrected. While the modeling tools based on PF solution have been extensively used by the oil and gas industry, certain assumptions may be violated with the smaller dimension and larger motion of a floating wind system.

A proposed approach is to tune the QTF using either tank-test data or a higher-fidelity modeling tool, such as computational fluid dynamics (CFD). One difficulty with this approach is that inviscid wave loading and viscous effects cannot be clearly separated because viscous effects can alter wave radiation characteristics, especially at small scale. Therefore, should the QTF be tuned based on experiment or CFD, no Morison drag can be included so as not to double-count viscous drag. Instead, an external damping matrix can be tuned to capture the free-decay characteristics. Another group within OC6 is

currently working on CFD analysis of the system and investigating how it can be used to better tune the engineering models, with a focus on understanding the low-frequency excitation using bichromatic waves. Results from this study are expected in the next year.

All data and simulation results from the OC6 project can be found after the conclusion of the work at the website: <https://a2e.energy.gov/projects/oc6>.

References

- [1] Robertson, A., et al. (2017). OC5 Project Phase II: Validation of global loads of the DeepCwind floating semisubmersible wind turbine, *Energy Procedia*, **137**, pp. 38-57. [DOI: [10.1016/j.egypro.2017.10.333](https://doi.org/10.1016/j.egypro.2017.10.333)]
- [2] Azcona, J., Bouchotrouch, F., and Vittori, F. (2019). Low-frequency dynamics of a floating wind turbine in wave tank-scaled experiments with SiL hybrid method. *Wind Energy*, **22**, pp. 1402-1413. [DOI: [10.1002/we.2377](https://doi.org/10.1002/we.2377)]
- [3] Pegalajar-Jurado, A., Bredmose, H., (2019). Reproduction of slow-drift motions of a floating wind turbine using second-order hydrodynamics and Operational Modal Analysis. *Marine Structures*, **66**, pp. 178-196. [DOI: [10.1016/j.marstruc.2019.02.008](https://doi.org/10.1016/j.marstruc.2019.02.008)]
- [4] Simos, A. N., Ruggeri, F., Watai, R. A., Souto-Iglesias, A., and Lopez-Pavon, C. (2018). Slow-drift of a floating wind turbine: An assessment of frequency-domain methods based on model tests. *Renewable Energy*, **116**, pp. 133-154. [DOI: [10.1016/j.renene.2017.09.059](https://doi.org/10.1016/j.renene.2017.09.059)]
- [5] Caillé, F., Bozonnet, P., Perdrizet, T., Poirette, Y., and Melis, C. (2017). Model test and simulation comparison for an inclined-leg TLP dedicated to floating wind. *Proceedings of the ASME 2017 36th International Conference on Ocean, Offshore and Arctic Engineering*.
- [6] Lemmer, F., et al. (2018). The TripleSpar campaign: Validation of a reduced-order simulation model for floating wind turbines. *Proceedings of ASME 37th International Conference on Ocean, Offshore and Arctic Engineering*.
- [7] Robertson, A., Bachynski, E., Gueydon, S., Wendt, F., and Schünemann, P. (2020). Total experimental uncertainty in hydrodynamic testing of a semisubmersible wind turbine, considering numerical propagation of systematic uncertainty, *Ocean Engineering*, **195**, pp. 106605. [DOI: [10.1016/j.oceaneng.2019.106605](https://doi.org/10.1016/j.oceaneng.2019.106605)]
- [8] Robertson, A., Mucha, P., Wendt, F., and Jonkman, J. (2020). OC6 Phase I definition document. *NREL Report*. [Forthcoming]
- [9] Jaouën, F., Koop, A., Vatinel, L. (2019). URANS predictions of low-frequency damping of a LNGC. *Proceedings of ASME 38th International Conference on Ocean, Offshore and Arctic Engineering*.
- [10] Berthelsen, P. A., Bachynski, E., Karimirad, M., and Thys, M. (2016). Real-time hybrid model tests of a braceless semisubmersible wind turbine. Part III: Calibration of a numerical model. *Proceedings of ASME 35th International Conference on Ocean, Offshore and Arctic Engineering*.

Acknowledgements

The authors would like to acknowledge the support of the MARINET2 project (European Union's Horizon 2020 grant agreement 731084), which supplied the tank test time and travel support to accomplish the testing campaign. The support of MARIN in the preparation, execution of the model-tests, and the evaluation of the uncertainties was essential for this study. MARIN's contribution was partly funded by the Dutch Ministry of Economic Affairs through TKI-ARD funding programs.

This work was authored in part by the National Renewable Energy Laboratory, operated by Alliance for Sustainable Energy, LLC, for the U.S. Department of Energy (DOE) under Contract No. DE-AC36-08GO28308. Funding provided by the U.S. Department of Energy Office of Energy Efficiency and Renewable Energy Wind Energy Technologies Office. The views expressed in the article do not necessarily represent the views of the DOE or the U.S. Government. The U.S. Government retains and the publisher, by accepting the article for publication, acknowledges that the U.S. Government retains a nonexclusive, paid-up, irrevocable, worldwide license to publish or reproduce the published form of this work, or allow others to do so, for U.S. Government purposes.

Appendix: Modeling Approach by Participant

Table A1. Potential Flow-Based Models

	Company Modeling Tool	Waves	BEM Geometry and QTF	Transverse Drag Coeff. ¹	Axial/Heave Drag Coeff. ^{1,2}	Additional Damping ³	Weak Nonlinearities
BVMO	Bureau Veritas Marine & Offshore (FR) Opera v0.1	Measured	Full geometry Full QTF	0.63 (all members)	LC2: 4.8 LC3-5: 5.76	Axial damping on moorings: 1.1E5 N/(m/s) $B_{55} = 9.5E9$	Instantaneous position
DENG	Doris Group OrcaFlex v10.3a	Synthesized	No bracing QTF (Newman's Approx.)	LC2&3: 1.4 (BC), 0.4 (others) LC4&5: 1.55 (BC), 0.4 (others)	LC2&3: 4.8 LC4&5: 3.0	$B_{11}=1.0E5, B_{33}=1.8E5, B_{55} = 7.5E7$	Instantaneous position
DNVG	DNV GL Bladed 4.9.0.21	Measured	Full geometry QTF (no bracing)	1.55 (BC), 0.325 (others)	3.57	None	Instantaneous position Excitation phase correction
DTU2	Tech. Univ. Denmark HAWC2 12.7	Measured	Full geometry Full QTF	1.52 (BC), 0.95 (others)	LC3-5: 2.4	$B_{11}=4.5E4, B_{33}=2.5E4$	Instantaneous position
DUT2	Dalian Univ. of Tech. OpenFAST v1.0.0	Measured	Full geometry QTF (no bracing)	1.3 (BC), 0.4 (others)	4.5	None	None
EDFR	EDF R&D DIEGO	Synthesized	Full geometry No QTF	LC2&3: 1.32 (BC), 0.44 (others) LC4&5: 2.0 (BC), 1.5 (others)	4.8 (BC) 4.0 (MC)	None	Nonlinear hydrostatics Instantaneous position
EDF2	Same as EDFR	Synthesized	Same as EDFR	LC4&5: 1.0 (BC), 1.5 (others)	Same as EDFR	$B_{11}=1.0E5, B_{33}=1.0E5$	Same as EDFR
FSUB	4Subsea OrcaFlex v10.3	Synthesized	Full geometry QTF (no bracing, Newman's Approx.)	1.5 (BC), 0.4 (others)	LC3-5: 4.8	None	Instantaneous position
IPDL	IFP Energies nouvelles PRINCIPIA DeepLines Wind V5.5.1	Measured	Full geometry QTF (no bracing, diff. freq. only)	1.5 (BC), 0.4 (others)	4.81	$B_{11}=B_{22}=75000$ $B_{44}=B_{55}=3.1E7$	Nonlinear hydrostatics
NREL	NREL OpenFAST v1.0.0	Measured	Full geometry Full QTF	1.6 (BC), 0.4 (others)	8.2	$B_{11}=7.5E4, B_{55}=3.1E7$	None
NTNU	NTNU SIMA v.3.6	Measured	No bracing Full QTF (diff. freq. only)	0.774 (all members)	2.483	$B_{11}=1.0E5, B_{33}=1.5E5, B_{55}=7.5E7$	None
QUBI	Queen's Univ. Belfast FlexCom V8.12.1	Load Case Dependent	Full geometry No QTF	0.82 (BC), 0.73 (UC), 0.67 (MC)	0.033	None	Instantaneous position
TECN	Tecalia OrcaFlex v10.2c	Measured	Full geometry No QTF	1.6 (BC), 0.35 (others)	None	None	Instantaneous position
TUHI	Hamburg Univ. of Tech. panMARE	Synthesized	No bracing (Pot.-flow solved at every time step)	1.25 (BC), 0.48 (UC), 0.44 (MC), 0.5 (bracing)	4.8	None	Nonlinear hydrostatics Instantaneous position
TUH3	Same as TUH1	Measured	Same as TUH1	Same as TUH1	Same as TUH1	Same as TUH1	Same as TUH1
UNEW	Newcastle Univ. DARwind v2.0	Synthesized	Full geometry No QTF	1.0 (bracing), 0.8 (others)	8.0	None	None
UOU1	Univ. of Ulsan FAST8 v16	Measured	No bracing No QTF	0.77 (MC), 0.46 (bracing), 0.78 (others)	4.8	$B_{11}=7.8E4, B_{33}=5.0E4, B_{55}=3.0E7$	None
UPC2	Univ. Poli. Catalunya FloaWDyn	Measured	No MC and bracing No QTF	Re-dependent pressure coeff. used instead of drag coeff..	1.29	$B_{11}=1.0E5, B_{55}=2.1E4$	Nonlinear hydrostatics for MC+braces only & inst. pos.
USTU	Univ. Stuttgart SLOW	Measured	Full geometry QTF (Newman's Approx.)	0.6 (all members)	LC3-5: 10	None	None
VULC	Vulcain OpenFAST	Measured	Full geometry Full QTF	1.6 (BC), 0.4 (others)	4.8	$B_{11}=7.0E4, Q_{11}=4.0E5, B_{55}=5.0E4$	None
WSIM	Sandia National Lab WEC-Sim	Measured	Full geometry No QTF	4.0 (all members)	7.8	Drag coefficients on mooring line (0.1m diameter): 1.17 (transverse), 0.05 (axial)	None
ZHJU	Zhejiang Univ. OpenFAST v2.2.0	Measured	Full geometry Full QTF	LC3-5: 1.5 (BC), 0.38 (others)	LC3-5: 7.8	$B_{11}=5.0E4, B_{55}=3.0E7$	None

1. UC and BC refer to the Upper Column and Base Column (heave plate) of the three corner columns. MC refers to the central Main Column.
2. Axial/heave drag is only applied on the bottom face of the heave plate or main column. Reference area for the drag coefficient is always the bottom surface area of the corresponding member. Unless specified otherwise, axial/heave drag is only applied to the heave plate / base column (BC) of the three corner columns.
3. Units for linear damping coefficients B_{11} (B_{33}) and B_{55} are N/(m/s) and Nm/(rad/s), respectively. Unit for quadratic damping coefficient Q_{11} is N/(m/s)².

Table A2. Morison's Equation-Only Models

	Company Modeling Tool	Waves	Transverse Added Mass Coeff. ¹	Axial/Heave Added Mass Coeff. ¹	Transverse Drag Coeff. ¹	Axial/Heave Drag Coeff. ^{1,2}	Additional Damping ³	Weak Nonlinearities
BVEX	Bureau Veritas (FR) Sancef Wind Turbines SWT18	Synthesized	0.63 (all members) MacCamy-Fuchs load model	2.6 Top/bottom of BC, Ref. Vol. 4m × top/bottom area	0.61 (UC), 0.68 (BC), 0.56 (MC), 0.63 (bracing)	2.4 Top/bottom of BC	None	Nonlinear hydrostatics and F-K forces Instantaneous pos.
CLNK	ClassNK NK-UTWind 6.0.0	Measured	0.5 (BC), 0.8 (UC), 1.5 (bracing)	Information not provided	0.4 (UC), 1.38 (BC)	4.2 Bottom of BC	$B_{11}=1.4E4$	Nonlinear hydrostatics and F-K forces Instantaneous pos.
DTU1	Tech. Univ. Denmark HAWC2 12.7 with fully nonlinear wave kinematics from OceanWave3D	Measured	LC2: 0.8-0.64 (BC), 0.47-0.72 (others) LC4: 0.52 (all memb.) LC3&5: 0.25 (BC), 1.48 (others)	LC4: 0.69 LC3&5: 0.64 Bottom of BC Ref. Vol: Equivalent hemisphere	LC2: 2.2 (BC), 0.5-1.1 (others) LC4: 0.35 (all members) LC3&5: 1.0 (BC), 1.5 (others)	LC4: 2.05 LC3&5: 2.4 Bottom of BC	$B_{11}=5.6E4, B_{33}=3.0E5, B_{55}=1.0E10$	Instantaneous pos.
IWES	Fraunhofer IWES MoWiT	Synthesized	0.63 (all members) MacCamy-Fuchs load model	1.0 Bottom of BC Ref. Vol. 4878.05 m ³	0.61 (UC), 0.68 (BC), 0.56 (MC), 0.63 (bracing)	4.8 Bottom of BC	None	Nonlinear F-K forces Instantaneous pos.
UPC1	Univ. Poli. Catalunya FloaWDyn	Measured	0.5 (all members) MacCamy-Fuchs load model	0.72 Top/bottom of BC, bot. of MC Ref. Vol: Equivalent hemisphere	1.5 (BC), 0.36 (others)	2.0 Top/bottom of BC and bottom of MC	$B_{11}=6.7E4, B_{33}=8.8E3, B_{55}=6.6E7$	Nonlinear hydrostatics Instantaneous pos.
UROS	Univ. Rostock OpenFAST v1.0.0	Measured	0.63 (all members)	1.540/1.348 Top/Bottom of BC Ref. Vol: Equivalent hemisphere	1.3 (BC), 0.43 (others)	4.8 Top/bottom of BC	$B_{11}=8.0E5$	None

1. UC and BC refer to the Upper Column and Base Column (heave plate) of the three corner columns. MC refers to the central Main Column.
2. Reference areas of axial/heave drag coefficients are the areas of the corresponding faces.
3. Units for linear damping coefficients B_{11} (B_{33}) and B_{55} are N/(m/s) and Nm/(rad/s), respectively.